

# Multi-Scale Markov-Switching GARCH: Volatility Regime Detection in EUR/USD

Jayesh Chaudhary  
Independent Researcher

May, 2026

## Abstract

Financial time series exhibit pronounced non-stationarity, rendering single-regime volatility models structurally misspecified for foreign exchange markets. This paper introduces a triple-timeframe Markov-Switching GARCH (MS-GARCH) framework with time-varying transition probabilities (TVTP) for volatility regime detection in EUR/USD, operating simultaneously across daily (1D Macro), four-hourly (4H Meso), and hourly (1H Micro) timescales. Each layer uses an AR(1)-MS-GARCH model with skewed Student-t emissions and three hidden states: Calm, Turbulent, and Crisis. These states are estimated through penalized maximum likelihood using Numba-JIT compiled Hamilton filter kernels. We build a 27-dimensional joint probability tensor as the outer product of the three marginal state probability vectors, and use this tensor to route signals through a Mixture-of-Experts architecture of 27 independent RidgeCV models.

The framework is evaluated on EUR/USD data spanning 2015–2025, with a strictly out-of-sample (OOS) period of 2021–2025 comprising 31,152 hourly observations across 16 walk-forward analysis (WFA) quarters. Key empirical results are as follows. The Diebold–Mariano test confirms statistically superior volatility forecasting relative to a GARCH(1,1) benchmark:  $DM = +4.7040$  ( $p = 1.28 \times 10^{-6}$ ). Kolmogorov–Smirnov distributional purity tests yield  $p = 1.35 \times 10^{-153}$  (Calm vs. Turbulent), confirming that the three regimes represent distinct data-generating processes. The smoothed Spearman information coefficient improves from 0.5264 (GARCH) to 0.5371 (MS-GARCH). TVTP is strongly justified at the 4H and 1H scales ( $\Delta AIC = +690.7$  and  $+499.9$  respectively), while the 1D model correctly employs a static specification. All three timescales preserved monotonic volatility ordering out-of-sample (Calm < Turbulent < Crisis), confirming statistically distinct regime separation. The out-of-sample directional information coefficient from the RidgeCV evaluation layer is  $+0.0252$  ( $p = 6.75 \times 10^{-5}$ ). The framework is positioned as a risk management tool rather than a standalone alpha engine.

**Keywords:** Markov-switching GARCH; regime detection; time-varying transition probabilities; EUR/USD; volatility forecasting; hidden Markov model; multi-scale analysis; walk-forward analysis

## Contents

### 1 Introduction

4

<b>2</b>	<b>Literature Review</b>	<b>5</b>
<b>3</b>	<b>Mathematical Foundations</b>	<b>7</b>
3.1	Hidden Markov Model Specification . . . . .	7
3.2	AR(1)-MS-GARCH Emission Model . . . . .	8
3.3	Time-Varying Transition Probabilities . . . . .	9
3.4	Penalised Maximum Likelihood Estimation . . . . .	10
3.5	Shannon Entropy and Regime Uncertainty . . . . .	11
<b>4</b>	<b>Data and Feature Engineering</b>	<b>11</b>
<b>5</b>	<b>Model Architecture</b>	<b>12</b>
<b>6</b>	<b>Multi-Scale Architecture and Walk-Forward Analysis</b>	<b>13</b>
6.1	The Scale Mismatch Problem . . . . .	13
6.2	Three-Layer Information Hierarchy . . . . .	13
6.3	Rolling Walk-Forward Analysis . . . . .	14
<b>7</b>	<b>Statistical Validation</b>	<b>14</b>
7.1	Transition Matrix Analysis . . . . .	14
7.2	Regime Classification Measure . . . . .	15
7.3	Brier Skill Scores . . . . .	15
7.4	ARCH-LM Residual Diagnostics . . . . .	15
7.5	TVTP Value Test . . . . .	16
7.6	VaR Breach Rate . . . . .	16
7.7	Consolidated Validation Scorecard . . . . .	16
<b>8</b>	<b>Volatility Forecasting Benchmark</b>	<b>16</b>
<b>9</b>	<b>Empirical Results</b>	<b>17</b>
9.1	Out-of-Sample Regime Allocations . . . . .	17
9.2	Conditional Return Profiles . . . . .	18
9.3	OOS Regime Validation Diagnostics . . . . .	18
9.4	Three-Dimensional Volatility Tensor . . . . .	20
9.5	Shannon Entropy Filter . . . . .	20
9.6	Formal Hypothesis Tests . . . . .	20
<b>10</b>	<b>Limitations and Future Research</b>	<b>21</b>

10.1 Residual ARCH Effects . . . . .	21
10.2 RCM Value . . . . .	21
10.3 Batch MLE: No Real-Time Adaptation . . . . .	21
10.4 Univariate Framework . . . . .	22
10.5 Markov Assumption and Duration Dependence . . . . .	22
10.6 Single Currency Pair . . . . .	22
<b>11 Conclusion</b>	<b>22</b>
<b>A Key Model Parameters and Diagnostic Statistics</b>	<b>25</b>
<b>B Formal Hypothesis Test Results</b>	<b>25</b>
<b>C WFA Quarterly Scorecard</b>	<b>26</b>

## 1. Introduction

Financial time series are characterised by pronounced non-stationarity: the statistical properties of asset returns—their mean, variance, autocorrelation structure, and tail behaviour—shift systematically across different market environments. Central bank policy cycles, geopolitical shocks, and liquidity crises create structural breaks that render single-regime models fundamentally misspecified. The canonical GARCH(1,1) model of Bollerslev (1986), while enormously influential, assumes a single data-generating process operating throughout the sample. When applied to EUR/USD returns over the 2021–2025 period, this assumption produces a notable result: the estimated ARCH coefficient  $\hat{\alpha} = 0.3038$  is three to six times above the typical range of 0.05–0.10 for foreign exchange data, with  $\hat{\beta} = 0.6076$  and total persistence  $\hat{\alpha} + \hat{\beta} = 0.9114$ . This anomalously high  $\hat{\alpha}$  is consistent with model misspecification arising from the imposition of a single-regime structure on a non-stationary process. A single-regime GARCH model, confronted with a sample that contains multiple structural regimes, absorbs the regime-switching dynamics into its shock-response parameter, becoming hyper-reactive to individual shocks in order to compensate for the absence of state-dependent variance paths.

An influential solution to this problem was provided by Hamilton (1989), whose Markov-switching framework introduced the concept of latent regime states governed by a first-order Markov chain. Hamilton’s model demonstrated that economic time series could be parsimoniously characterised as switching between a small number of distinct data-generating processes, with the switching mechanism itself being probabilistically estimated from the data. The subsequent development of Markov-Switching GARCH (MS-GARCH) models, pioneered by Gray (1996) and refined by Haas et al. (2004), extended this framework to accommodate state-dependent volatility dynamics. The Haas et al. (2004) specification, which runs  $K$  independent parallel GARCH processes—one per regime—is particularly tractable because it avoids the path-dependence explosion that afflicts the Gray (1996) integrated formulation.

Despite this progress, existing MS-GARCH implementations share a common limitation: they operate at a single timescale. This is a structural misspecification for foreign exchange markets, where regime dynamics are hierarchically nested across multiple temporal scales. A central bank policy shift (a macro regime change) unfolds over months; an institutional positioning cycle (a meso regime change) unfolds over days; a liquidity-driven intraday stress event (a micro regime change) unfolds over hours. These three classes of dynamics are simultaneously present in any EUR/USD hourly return series, yet they are governed by fundamentally different data-generating processes. A single-scale HMM fitted to hourly data faces a fundamental modelling challenge: its transition matrix must simultaneously encode the very low off-diagonal probabilities appropriate for macro regime transitions ( $P[\text{Calm} \rightarrow \text{Crisis}] \approx 0.001$  per day) and the higher off-diagonal probabilities appropriate for intraday microstructure transitions ( $P[\text{Calm} \rightarrow \text{Turbulent}] \approx 0.08$  per hour). These requirements place conflicting demands on a single  $K \times K$  transition matrix.

This paper makes three core contributions to the literature on volatility regime detection:

- 1. Multi-Scale MS-GARCH architecture:** We introduce a framework that fits three

independent AR(1)-MS-GARCH models simultaneously at the 1D Macro, 4H Meso, and 1H Micro timescales, each optimised for the dynamics at its native scale. The outputs are combined through a 27-dimensional joint probability tensor  $\mathcal{P}_t(i, j, k) = \pi_t^{(1D)}(i) \times \pi_t^{(4H)}(j) \times \pi_t^{(1H)}(k)$ , enabling cross-scale interaction analysis that is not available in single-timeframe models.

**2. Time-varying transition probabilities with composite stress drivers:** We implement the Filardo (1994) multinomial logit TVTP specification, driven by composite microstructure stress indices constructed from volatility z-scores, spread proxies, and momentum signals. TVTP is strongly justified at the 4H and 1H scales ( $\Delta\text{AIC} = +690.7$  and  $+499.9$ ) (Akaike, 1974), while the 1D model correctly employs a static specification (positive AIC =  $+2170.24$  suggests near-overparameterisation on 1,871 daily bars).

**3. Cross-scale probability tensor for state-dependent prediction and Shannon entropy filtering:** The joint probability tensor serves as soft routing weights for 27 independent RidgeCV expert models, each specialised for a specific (Macro, Meso, Micro) regime combination. A Shannon entropy filter (Shannon, 1948) suppresses trading during high-uncertainty environments.

The empirical evaluation employs EUR/USD 1-minute mid-price data from 2015 to 2025, resampled to 1H, 4H, and 1D frequencies. The out-of-sample period spans 2021-01-01 to 2025-01-01, comprising 31,152 hourly observations across 16 walk-forward analysis quarters (2021-Q1 through 2024-Q4). The WFA protocol employs a rolling 5-year training window of approximately 31,000 hourly bars, with a rolling training scheme that avoids cold-start discontinuities across quarter boundaries.

## 2. Literature Review

The intellectual lineage of this paper begins with Hamilton (1989), whose seminal contribution introduced the Markov-switching model as a framework for characterising non-stationary economic time series. Hamilton demonstrated that US GNP growth could be parsimoniously described as switching between two distinct data-generating processes—expansion and contraction—governed by a first-order Markov chain. The forward-backward algorithm he developed for computing filtered and smoothed state probabilities has  $O(TK^2)$  computational complexity and remains the standard inference procedure for hidden Markov models (Hamilton, 1989). The key insight of Hamilton (1989) is that the latent state sequence need not be observed directly; it can be inferred probabilistically from the observable data through the recursive Hamilton filter.

The parallel development of GARCH models by Bollerslev (1986), building on the ARCH framework of Engle (1982), provided the standard toolkit for modelling conditional heteroskedasticity in financial time series. The GARCH(1,1) model captures two fundamental stylised facts of financial volatility: volatility clustering (periods of high volatility tend to be followed by high volatility) and mean reversion (volatility eventually returns to its unconditional level). However, as Bollerslev (1986) himself acknowledged, the GARCH framework assumes a single, stationary data-generating process. When applied to samples containing structural breaks, the GARCH model absorbs the non-stationarity into its parameters, producing the anomalously high ARCH

coefficients documented in this paper.

The integration of Markov-switching dynamics with GARCH volatility models was first attempted by Gray (1996), who proposed an MS-GARCH specification in which the conditional variance depends on the full history of regime-weighted variances. Gray (1996) proposed a “collapsing” approximation that reduces the path count at each step, but this approximation introduces bias and increases computational cost by a factor of 3–5 relative to simpler specifications.

A computationally tractable alternative was proposed by Haas et al. (2004), who proposed running  $K$  independent parallel GARCH processes (one per regime) and switching between them according to the Markov chain. The Haas et al. (2004) specification makes the likelihood exactly tractable because each regime’s variance path depends only on the within-regime history, not on the full cross-regime history. This is the specification adopted in the present paper. The independence assumption introduces a known limitation: the within-state GARCH does not condition on volatility inherited from previous states, but this is a worthwhile trade-off for computational tractability, particularly in the multi-timeframe setting where three separate models must be estimated.

The extension of MS-GARCH to time-varying transition probabilities was pioneered by Filardo (1994), who demonstrated that business cycle transition probabilities could be modelled as functions of leading economic indicators through a multinomial logit specification. Filardo (1994) showed that allowing transition probabilities to vary with observable covariates substantially improved the model’s ability to predict regime transitions in advance, rather than merely detecting them contemporaneously. This insight is directly applicable to foreign exchange markets, where microstructure stress indices, constructed from volatility z-scores, spread proxies, and momentum signals provide genuine leading information about regime transitions.

Recent developments in the MS-GARCH literature have focused on improving both distributional flexibility and estimation methodology. Alternative heavy-tailed emission distributions, including Normal Inverse Gaussian (NIG) and Variance Gamma (VG) specifications, have been proposed to better capture extreme market movements and asymmetric tail behaviour. In parallel, Bayesian estimation methods, Markov Chain Monte Carlo techniques, and Sequential Monte Carlo approaches have been developed to address inference challenges and enable more adaptive state estimation.

Despite these advances, much of the literature continues to focus on modelling regime dynamics at a single temporal resolution. The present study extends this literature by jointly modelling regime dynamics across daily, four-hour, and hourly horizons and integrating the resulting state probabilities into a unified cross-scale probability tensor. This multi-scale architecture enables the analysis of regime interactions across temporal horizons rather than treating each timescale in isolation.

The evaluation of competing volatility forecasts requires a formal statistical test. Diebold and Mariano (1995) developed the Diebold–Mariano (DM) test, which tests the null hypothesis of equal predictive accuracy between two forecasting models using the loss differential  $d_t = L(e_{1t}) - L(e_{2t})$ , where  $L(\cdot)$  is a loss function (typically squared error) and  $e_{it}$  is the forecast error of model  $i$ . Under the null, the DM statistic  $\bar{d}/\sqrt{\hat{\sigma}_d^2/T}$  is asymptotically standard normal. A positive DM

statistic indicates that model 1 has smaller average loss than model 2. The DM test is the appropriate tool for comparing the MS-GARCH and GARCH(1,1) volatility forecasts in this paper.

The probabilistic calibration of regime probability forecasts is assessed using the Brier Score of Brier (1950), which measures the mean squared error of probabilistic forecasts for binary events. The Brier Skill Score (BSS) compares the model’s Brier Score to that of a climatological reference forecast, with  $BSS > 0$  indicating skill above the base rate. The BSS is particularly appropriate for evaluating crisis probability forecasts, where the base rate is low (2–8% depending on the timeframe) and the cost of false negatives is high.

The residual diagnostics employ the ARCH-LM test of Engle (1982), which tests for remaining conditional heteroskedasticity in the standardised residuals after model fitting. Rejection of the null hypothesis of no ARCH effects indicates that the within-state GARCH specification has not fully captured the volatility clustering dynamics, motivating extensions to higher-order GARCH or asymmetric specifications.

The Markov assumption underlying all HMM specifications implies that regime transitions depend only on the current state, not on how long the system has been in that state. Durland and McCurdy (1994) documented empirical evidence of duration dependence in US GNP growth regimes, motivating semi-Markov models in which transition probabilities depend on regime age. This limitation is acknowledged in Section 10.

### 3. Mathematical Foundations

#### 3.1 Hidden Markov Model Specification

Let  $\{S_t\}_{t=1}^T$  denote a latent Markov chain taking values in the state space  $\mathcal{S} = \{0, 1, 2\}$ , corresponding to the Calm, Turbulent, and Crisis regimes respectively. The chain is characterised by an initial distribution  $\pi_0 = (\pi_0(0), \pi_0(1), \pi_0(2))^\top$  with  $\sum_k \pi_0(k) = 1$ , and a  $K \times K$  transition matrix  $P = [p_{ij}]$  where

$$p_{ij} = P(S_t = j \mid S_{t-1} = i), \quad \sum_{j=0}^{K-1} p_{ij} = 1 \quad \forall i. \quad (1)$$

The first-order Markov property states that  $P(S_t \mid S_{t-1}, S_{t-2}, \dots, S_1) = P(S_t \mid S_{t-1})$ , so the full history of the chain is summarised by the current state. The observable return series  $\{r_t\}$  is conditionally independent given the state sequence:  $r_t \perp r_s \mid S_t$  for  $t \neq s$ .

The Hamilton filter (Hamilton, 1989) computes the filtered state probabilities  $\xi_{t|t}(k) = P(S_t = k \mid r_1, \dots, r_t)$  recursively. The prediction step propagates the previous filtered probabilities through the transition matrix:

$$\xi_{t|t-1}(j) = \sum_{k=0}^{K-1} p_{kj} \cdot \xi_{t-1|t-1}(k), \quad (2)$$

and the update step incorporates the new observation:

$$\xi_{t|t}(k) = \frac{f(r_t | S_t = k, \theta_k) \cdot \xi_{t|t-1}(k)}{\sum_{j=0}^{K-1} f(r_t | S_t = j, \theta_j) \cdot \xi_{t|t-1}(j)}, \quad (3)$$

where  $f(r_t | S_t = k, \theta_k)$  is the emission density for state  $k$  with parameters  $\theta_k$ . The log-sum-exp trick is applied in the denominator to prevent numerical underflow:  $\log \sum_j \exp(a_j) = \max_j a_j + \log \sum_j \exp(a_j - \max_j a_j)$ . The Hamilton filter has  $O(TK^2)$  computational complexity, which is manageable for  $K = 3$  and  $T \leq 40,000$ .

### 3.2 AR(1)-MS-GARCH Emission Model

The return equation incorporates an AR(1) mean specification to capture the well-documented first-order autocorrelation in high-frequency FX returns:

$$r_t = \mu_{S_t} + \phi_{S_t} r_{t-1} + \varepsilon_t, \quad (4)$$

where  $\mu_{S_t}$  is the state-dependent intercept and  $\phi_{S_t}$  is the state-dependent AR(1) coefficient. The residual  $\varepsilon_t$  follows a state-dependent GARCH(1,1) process:

$$\sigma_{t,k}^2 = \omega_k + \alpha_k \varepsilon_{t-1}^2 + \beta_k \sigma_{t-1,k}^2, \quad (5)$$

where  $\omega_k > 0$ ,  $\alpha_k \geq 0$ , and  $\beta_k \geq 0$  are state-specific parameters and  $\varepsilon_{t-1}$  denotes the innovation from the conditional mean equation. Following Haas et al. (2004), all regime-specific variance processes are updated using the same realized return innovation while each state maintains its own conditional variance dynamics. The unconditional variance within state  $k$  is:

$$\sigma_{k,\infty}^2 = \frac{\omega_k}{1 - \alpha_k - \beta_k}, \quad (6)$$

which requires the covariance stationarity condition  $\alpha_k + \beta_k < 1$  for all  $k$ .

Following Haas et al. (2004), the  $K$  GARCH processes run independently in parallel, one per regime. This contrasts with the Gray (1996) path-dependent specification, in which the variance at time  $t$  depends on the probability-weighted average of all past regime-specific variances. The Haas et al. (2004) specification is adopted here because it makes the likelihood exactly tractable and reduces computational cost by a factor of 3–5x relative to the Gray (1996) collapsing approach.

The emission distribution is a standardised Student- $t$  with state-specific degrees of freedom  $\nu_k$ :

$$\log f(\varepsilon_t; \sigma_{t,k}, \nu_k) = \log \Gamma\left(\frac{\nu_k + 1}{2}\right) - \log \Gamma\left(\frac{\nu_k}{2}\right) - \frac{1}{2} \log[\pi(\nu_k - 2)] - \log \sigma_{t,k} - \frac{\nu_k + 1}{2} \log \left[ 1 + \frac{(\varepsilon_t / \sigma_{t,k})^2}{\nu_k - 2} \right]. \quad (7)$$

The model employs staggered parameter bounds designed to encourage economically interpretable regime separation and mitigate label switching during estimation. The constraints

enforce the economically motivated ordering Calm < Turbulent < Crisis in volatility and tail-risk characteristics.

These bounds are implemented as box constraints within the L-BFGS-B optimiser. The stagger on  $\omega_k$  encourages higher baseline variance in higher-volatility regimes, while the stagger on  $\nu_k$  encourages heavier tails in Crisis states, consistent with observed financial market behaviour.

### 3.3 Time-Varying Transition Probabilities

Following Filardo (1994), the transition probabilities are modelled as functions of an observable composite stress index  $z_t$  through a multinomial logit specification:

$$p_{ij,t} = \frac{\exp(a_{ij} + \gamma_{ij}z_t)}{\sum_{k=0}^{K-1} \exp(a_{ik} + \gamma_{ik}z_t)}, \quad (8)$$

where  $a_{ij}$  are baseline log-transition parameters,  $\gamma_{ij}$  are TVTP sensitivity coefficients, and  $z_t$  is the standardized exogenous driver. The softmax structure guarantees  $\sum_j p_{ij,t} = 1$  for all  $i$  and  $t$ . The sensitivity coefficients are estimated subject to box constraints to prevent the exogenous driver from dominating the baseline transition structure and to preserve stable Markov dynamics during optimization.

The composite stress driver  $z_t$  is constructed using timeframe-specific feature compositions. For the 1H Micro model,

$$z_t^{(1H)} = 0.80 \cdot \text{comp\_meta\_1h\_z} + 0.10 \cdot \text{DOW\_Seasonality} + 0.10 \cdot \text{Hour\_Seasonality},$$

where  $\text{comp\_meta\_1h\_z}$  is the standardized microstructure stress signal

$$\text{comp\_meta}_{1H} = \text{MicroVolSpike} \times \log(1 + \text{JumpRatio}),$$

combining intraday volatility acceleration with jump activity and subsequently standardized via a rolling 30-day z-score.

For the 4H Meso model,

$$z_t^{(4H)} = 0.60 \cdot \text{comp\_meta\_4h\_z} + 0.25 \cdot \text{DOW\_Seasonality} + 0.15 \cdot \text{Macro\_Stress\_Index},$$

where  $\text{comp\_meta\_4h\_z}$  is a standardized meso-scale stress signal combining volatility acceleration and jump activity over a rolling 120-hour horizon. The Macro Stress Index is defined as

$$\text{Macro\_Stress\_Index} = \text{VIX\_Z} + \text{Yield\_Z},$$

where both components are rolling 30-day z-scores of the VIX and US 10-year Treasury yield, shifted by one period to enforce strict causality.

TVTP model selection employs the Akaike Information Criterion,

$$\text{AIC} = 2k - 2 \log \hat{L},$$

where  $k$  denotes the number of free parameters and  $\hat{\mathcal{L}}$  is the maximized likelihood. The TVTP specification introduces an additional  $K^2 = 9$  sensitivity parameters  $\gamma_{ij}$  relative to the static model. The improvement criterion is defined as

$$\Delta\text{AIC} = \text{AIC}_{\text{static}} - \text{AIC}_{\text{TVTP}}.$$

A  $\Delta\text{AIC}$  greater than 10 is generally interpreted as strong evidence in favor of the TVTP specification. The empirical results are  $\Delta\text{AIC} = +690.7$  (4H),  $\Delta\text{AIC} = +499.9$  (1H), and  $\Delta\text{AIC} = -2170.24$  (1D), indicating strong support for time-varying transition dynamics at the meso and micro horizons, while providing evidence against the TVTP extension at the daily frequency.

### 3.4 Penalised Maximum Likelihood Estimation

The objective function minimised by the L-BFGS-B optimiser is the penalised negative log-likelihood:

$$\begin{aligned} \mathcal{L}_{\text{pen}}(\theta) = & -\log \mathcal{L}(\theta) + \sum_{k=0}^{K-1} \lambda_k (-\log p_{kk}) \\ & + \lambda_{\text{ord}} \sum_{k=0}^{K-2} \max(0, p_{k+1,k+1} - p_{k,k})^2 \\ & + \lambda_{\text{stat}} \sum_{k=0}^{K-1} \max(0, \alpha_k + \beta_k - 0.999)^2, \end{aligned} \quad (9)$$

where  $-\log \mathcal{L}(\theta)$  is the standard Hamilton filter negative log-likelihood. The second term is a log-Dirichlet stickiness prior with per-state weights  $\lambda_k$  (state-specific persistence penalties are employed, with larger penalties assigned to lower-volatility states in order to encourage realistic regime persistence), which penalises low diagonal persistence. An ordering penalty is imposed to discourage violations of the persistence hierarchy  $p_{00} \geq p_{11} \geq p_{22}$ . The fourth term is the GARCH stationarity penalty, which prevents explosive variance dynamics.

The L-BFGS-B optimiser is chosen for three reasons: the parameter space is high-dimensional (27 static or 36 TVTP parameters) but smooth; box constraints from the staggered bounds are natively supported; and the limited-memory Hessian approximation is computationally efficient at this parameter scale. The label-switching problem—the tendency of mixture model optimisers to permute state labels across runs—is resolved through variance-based state sorting: states are relabelled in ascending order of their empirical within-state return variance, ensuring that State 0 always corresponds to the lowest-variance (Calm) regime.

### 3.5 Shannon Entropy and Regime Uncertainty

The Shannon entropy of the filtered state probability vector provides a scalar measure of regime uncertainty:

$$H_t = - \sum_{k=0}^{K-1} \pi_t(k) \log \pi_t(k), \quad (10)$$

with maximum value  $\log K = \log 3 \approx 1.099$  for  $K = 3$  states. The normalised entropy is:

$$\tilde{H}_t = \frac{H_t}{\log K} \in [0, 1]. \quad (11)$$

The entropy threshold  $\tilde{H}_t > 0.85$  is used to identify high-uncertainty environments, preventing trading in the most uncertain regime environments.

## 4. Data and Feature Engineering

The primary dataset consists of EUR/USD 1-minute mid-price (bid-ask midpoint) data spanning 2015–2025. The data are resampled to three frequencies using strictly causal aggregation: 1H (last close of each hour), 4H (last close of each 4-hour bar), and 1D (last close of each trading day). Log returns are computed as:

$$r_t = \log(P_t/P_{t-1}) \times 100, \quad (12)$$

where the multiplication by 100 converts to percentage log returns, improving numerical conditioning for the GARCH parameter estimation. The train/test split date is 2021-01-01. The resulting dataset sizes are: 1D (1,871 train / 1,562 test bars), 4H (9,654 / 8,055), and 1H (37,345 / 31,152). The out-of-sample period comprises 31,152 hourly observations across 16 walk-forward analysis quarters.

The TVTP driver construction employs three layers of causal isolation to prevent look-ahead bias. First, all TVTP drivers use a one-period lag to prevent endogenous leakage. Second, the train/test split uses strict boundary slicing with a one-hour offset. Third, the maximum horizon trimming removes the last 24 training observations from the feature matrix to prevent multi-step forward target overlap.

The composite meta-signal is constructed as:

$$\text{composite\_meta} = \text{Vol\_Spike} \times \log(1 + \text{Jump\_Ratio}), \quad (13)$$

where  $\text{Vol\_Spike} = \sigma_{15\text{min}}/\sigma_{24\text{h}}$  is the ratio of 15-minute realised volatility to 24-hour baseline volatility, and  $\text{Jump\_Ratio} = \text{Realized\_Var}_{24\text{h}}/\text{Bipower\_Var}$  is the ratio of realised variance to bipower variation (a jump-robust estimator). The product combines simultaneous volatility spikes and jump activity, the hallmark of intraday crisis events. All composite signals are standardised via rolling 30-day z-scores and clipped to  $\pm 3\sigma$  to prevent outlier contamination.

The 27-expert Mixture-of-Experts feature matrix includes 47 features spanning mean reversion

signals, momentum signals, volatility regime indicators, derived HMM features including entropy measures, dwell-time statistics, confidence scores, forward crisis hazard estimates, and cross-scale disagreement metrics. The top feature by absolute WFA Ridge coefficient is "Sig\_MR" with coefficient +0.001086, consistent with EUR/USD's well-documented mean-reverting behaviour at the 1H scale.

## 5. Model Architecture

The implementation consists of an AR(1)-MS-GARCH framework integrated within a broader machine-learning pipeline.

The static specification contains 27 optimization parameters per timeframe: 18 state-conditional emission parameters  $\mu_k, \phi_k, \omega_k, \alpha_k, \beta_k, \nu_k$  for  $k \in \{0, 1, 2\}$  and 9 unconstrained transition parameters. The transition matrix is mapped to a row-stochastic probability matrix through a softmax normalization. Although the resulting transition matrix has only six statistical degrees of freedom, the optimization is performed in a 9-dimensional unconstrained parameter space for numerical stability.

For the TVTP specification, an additional 9 transition-sensitivity coefficients  $\gamma_{ij}$  are introduced, increasing the parameter count from 27 to 36 optimization parameters per timeframe. The Hamilton filter is implemented via Numba-JIT compiled kernels, achieving C-level execution speed. The log-sum-exp trick is applied throughout for numerical stability.

The stickiness prior vector for the 1H Micro model encodes the empirical prior that Calm regimes are highly persistent, Turbulent regimes are moderately persistent, and Crisis regimes are short-lived.

The 27-expert Mixture-of-Experts architecture constructs the joint probability tensor as:

$$\mathcal{P}_t(i, j, k) = \pi_t^{(1D)}(i) \times \pi_t^{(4H)}(j) \times \pi_t^{(1H)}(k), \quad i, j, k \in \{0, 1, 2\}, \quad (14)$$

implemented via `numpy.einsum` for computational efficiency. The resulting 27-dimensional vector is normalised to sum to 1 and serves as soft routing weights for the 27 independent RidgeCV expert models. Expert models are only trained when their state combination has at least 1,000 training observations; data-sparse combinations fall back to the global model. Forward-fill alignment propagates daily and 4H state probabilities to the hourly index using the unique causal method (forward-fill alignment), ensuring no look-ahead bias.

The Regime Disagreement metric captures cross-scale conflict:

$$\text{Disagreement}_t = \frac{1}{K} \sum_{k=0}^{K-1} \text{std} \left( \pi_t^{(1H)}(k), \pi_t^{(4H)}(k), \pi_t^{(1D)}(k) \right), \quad (15)$$

where the standard deviation is computed across the three timescales for each state  $k$ . High disagreement indicates that the three timescales are assigning different regime probabilities, which is itself an informative signal about regime uncertainty and transition risk.

## 6. Multi-Scale Architecture and Walk-Forward Analysis

### 6.1 The Scale Mismatch Problem

The fundamental motivation for the multi-scale architecture is the incompatibility of regime transition rates across timescales. At the daily frequency, macro regime transitions are rare:  $P[\text{Calm} \rightarrow \text{Crisis}] \approx 0.001$  per day, corresponding to a direct jump probability of 0.0215 in the estimated 1D transition matrix. At the hourly frequency, microstructure transitions are far more frequent:  $P[\text{Calm} \rightarrow \text{Turbulent}] \approx 0.08$  per hour, as reflected in the 1H transition matrix entry  $p_{01} = 0.0824$ . A single  $K \times K$  transition matrix cannot simultaneously encode both rates; the optimiser will find a compromise that satisfies neither constraint well.

Four independent arguments support the multi-scale architecture. The *computational argument* notes that a single HMM on 1H data with  $K = 9$  states (to capture  $3 \times 3$  macro-micro combinations) would have  $O(TK^2) = O(50,000 \times 81)$  complexity per likelihood evaluation, compared to three separate  $K = 3$  models with  $O(50,000 \times 9)$  each. The *statistical argument* notes that a single model must simultaneously capture dynamics at incompatible timescales, producing a misspecified transition matrix. The *interpretability argument* notes that the multi-scale architecture produces separately interpretable outputs at each scale. The empirical argument notes that the three models produce materially different regime allocations, persistence characteristics, and transition dynamics, indicating that each timescale captures distinct aspects of market behaviour.

### 6.2 Three-Layer Information Hierarchy

The three models capture distinct layers of market dynamics. The 1D Macro model captures macro-structural regime changes driven by central bank policy cycles, geopolitical risk episodes, and long-horizon capital flows. The 4H Meso model captures medium-term flow regimes driven by institutional positioning cycles, options expiry dynamics, and multi-day momentum. The 1H Micro model captures intraday microstructure regimes driven by session transitions, news flow, and short-term liquidity dynamics.

**Table 1:** Three-Layer Architecture: Comparative Summary

Dimension	1D Macro	4H Meso	1H Micro
Training bars	1,871	9,654	37,345
Test bars	1,562	8,055	31,152
TVTP specification	Static	$\Delta\text{AIC} = +690.7$	$\Delta\text{AIC} = +499.9$
AIC	+2170.24	-6880.72	-80160.25
Calm dwell time	45.1 days	10.8 days	10.7 hours
Turbulent dwell time	13.9 days	1.9 days	5.1 hours
Crisis dwell time	7.6 days	0.6 days	3.9 hours
OOS Calm allocation	82.3%	8.4%	65.6%
OOS Turbulent allocation	10.1%	71.6%	32.5%
OOS Crisis allocation	7.7%	20.0%	2.0%
Brier Skill Score	+0.2132	+0.0874	+0.1185
RCM Clarity	27.6%	52.4%	54.0%

The 4H Meso model’s Turbulent-dominant allocation (71.6%) is expected for EUR/USD during the 2021–2025 period, which was characterised by persistent institutional flow activity, elevated options market activity, and frequent ECB/Fed communication events. The 1D Macro model’s Calm-dominant allocation (82.3%) reflects the daily timescale’s lower sensitivity to intraday noise; at the daily level, EUR/USD spends most of its time in a low-volatility, mean-reverting regime.

### 6.3 Rolling Walk-Forward Analysis

The walk-forward analysis protocol employs 16 non-overlapping quarters from 2021-Q1 through 2024-Q4. At each quarter boundary, the three HMM models are re-estimated on a rolling 5-year window of approximately 31,000 hourly bars. The design fuses the training tail to the test head, ensuring that rolling features (such as 24-hour moving averages) roll seamlessly across quarter boundaries without introducing NaN values or look-ahead bias.

The warm start strategy initialises the L-BFGS-B optimiser at the parameter estimates from the previous quarter, rather than at the default initial guess. This provides three benefits: reduced optimisation time (starting close to the solution requires fewer iterations); improved label consistency (warm start anchors the solution near the previous quarter’s labelling, reducing label switching); and smooth tracking of gradual parameter drift (regime characteristics evolve slowly over time, and warm start allows the model to track this drift quarter-by-quarter).

The 16 quarters span a remarkably diverse set of macro environments: post-COVID recovery with EUR/USD ranging between 1.17 and 1.23 (2021); the Fed tightening cycle with EUR/USD declining to parity and Russia-Ukraine shock (2022); banking stress with SVB and Credit Suisse failures (2023); and carry trade unwind and normalisation (2024). This diversity provides a rigorous test of the model’s robustness across different market regimes.

## 7. Statistical Validation

### 7.1 Transition Matrix Analysis

Under the first-order Markov property, the expected dwell time in state  $k$  follows from the geometric distribution:

$$\mathbb{E}[T_k] = \frac{1}{1 - p_{kk}}. \quad (16)$$

The three estimated transition matrices are as follows. For the 1D Macro model (static):

$$P^{(1D)} = \begin{pmatrix} 0.9778 & 0.0007 & 0.0215 \\ 0.0025 & 0.9283 & 0.0693 \\ 0.0768 & 0.0548 & 0.8685 \end{pmatrix}, \quad (17)$$

yielding dwell times of 45.1 days (Calm), 13.9 days (Turbulent), and 7.6 days (Crisis). For the 4H Meso model (TVTP):

$$P^{(4H)} = \begin{pmatrix} 0.9846 & 0.0151 & 0.0003 \\ 0.0136 & 0.9125 & 0.0738 \\ 0.0177 & 0.2541 & 0.7282 \end{pmatrix}, \quad (18)$$

yielding dwell times of 10.8 days (Calm), 1.9 days (Turbulent), and 0.6 days (Crisis). For the 1H Micro model (TVTP):

$$P^{(1H)} = \begin{pmatrix} 0.9062 & 0.0824 & 0.0113 \\ 0.1437 & 0.8028 & 0.0535 \\ 0.0332 & 0.2228 & 0.7440 \end{pmatrix}, \quad (19)$$

yielding dwell times of 10.7 hours (Calm), 5.1 hours (Turbulent), and 3.9 hours (Crisis). The hierarchical structure is immediately apparent: macro regimes are slow-moving structural states, meso regimes are medium-frequency cyclical states, and micro regimes are high-frequency transient states.

## 7.2 Regime Classification Measure

The Regime Classification Measure (RCM) quantifies the sharpness of regime assignments:

$$\text{RCM} = 100 \times \left[ 1 - \frac{K}{K-1} \cdot \frac{1}{T} \sum_{t=1}^T \sum_{k=0}^{K-1} \pi_t(k)(1 - \pi_t(k)) \right]. \quad (20)$$

RCM = 100% indicates perfect classification (all probabilities are 0 or 1); RCM = 0% indicates uniform uncertainty. The empirical results are 27.6% (1D), 52.4% (4H), and 54.0% (1H). The values indicate moderate regime classification confidence, which is expected in FX markets where emission distributions overlap more than in equity markets.

## 7.3 Brier Skill Scores

The Brier Skill Score (Brier, 1950) measures probabilistic forecast skill relative to a climatological baseline:

$$\text{BSS} = 1 - \frac{\text{BS}_{\text{model}}}{\text{BS}_{\text{ref}}} = 1 - \frac{(1/T) \sum_t (p_t - y_t)^2}{\bar{p}(1 - \bar{p})}, \quad (21)$$

where  $p_t = \pi_t(\text{Crisis})$  is the model's crisis probability forecast and  $y_t = 1[|r_t| > 85\text{th percentile}]$  is the realised high-volatility indicator. The empirical results are +0.2132 (1D), +0.0874 (4H), and +0.1185 (1H). All three timeframes achieve positive BSS, confirming that the MS-GARCH model has genuine skill in predicting high-volatility periods beyond the climatological base rate.

## 7.4 ARCH-LM Residual Diagnostics

The ARCH-LM test (Engle, 1982) applied to the standardised residuals  $\hat{\varepsilon}_t = r_t / \sigma_{t, \hat{\sigma}_t}$  reveals persistent conditional heteroskedasticity in all three timeframes: LM = 12.19 ( $p = 0.032$ ) for

1D,  $LM = 16.75$  ( $p = 0.005$ ) for 4H, and  $LM = 38.49$  ( $p = 0.000$ ) for 1H. The residual ARCH is most severe at the 1H Micro level, which is expected given that intraday volatility clustering is stronger than daily clustering. The unconditional ACF of squared returns is 0.2579, reduced to a within-state maximum of 0.1889 by the MS-GARCH model, representing a 26.8% absorption of total volatility clustering. The residual ARCH is an acknowledged limitation addressed in Section 10.

### 7.5 TVTP Value Test

The TVTP value test (Akaike, 1974) compares the AIC of the TVTP model to the static model:  $\Delta AIC = AIC_{\text{static}} - AIC_{\text{TVTP}}$ . The empirical results confirm strong TVTP superiority at the 4H and 1H scales ( $\Delta AIC = +690.7$  and  $+499.9$ , far exceeding the threshold of 10 for decisive evidence), while the 1D model correctly employs a static specification (positive AIC =  $+2170.24$  confirms near-overparameterisation).

### 7.6 VaR Breach Rate

The 99% VaR breach rate is 0.54% versus the target of 1.00%, indicating that the model is conservative in its tail risk estimation. This is a desirable property for risk management applications: the model overestimates tail risk, providing a safety margin against unexpected extreme events.

### 7.7 Consolidated Validation Scorecard

**Table 2:** Consolidated Statistical Validation Scorecard

Test	1D Macro	4H Meso	1H Micro
Ordering constraint	Valid	Valid	Valid
RCM Clarity	27.6%	52.4%	54.0%
Brier Skill Score	+0.2132	+0.0874	+0.1185
ARCH-LM $p$ -value	0.032	0.005	0.000
TVTP $\Delta AIC$	N/A (static)	+690.7	+499.9
VaR 99% breach rate	0.54%	—	—
Label integrity (OOS)	Monotonic	Monotonic	Monotonic

## 8. Volatility Forecasting Benchmark

The GARCH(1,1) benchmark (Bollerslev, 1986) is estimated on the training set using maximum likelihood, yielding parameters  $\hat{\omega} = 0.001680$ ,  $\hat{\alpha} = 0.3038$ ,  $\hat{\beta} = 0.6076$ , and persistence  $\hat{\alpha} + \hat{\beta} = 0.9114$ . The anomalously high  $\hat{\alpha} = 0.3038$ —three to six times above the typical range of 0.05–0.10 for EUR/USD—is a diagnostic signature of model misspecification. The single-regime GARCH model, confronted with a sample containing multiple structural regimes, absorbs the regime-switching dynamics into its shock-response parameter. The relatively low  $\hat{\beta} = 0.6076$  (compared

to typical values of 0.85–0.92) is the counterpart: the combination of high  $\hat{\alpha}$  and low  $\hat{\beta}$  creates a model that reacts aggressively to individual shocks but does not sustain elevated volatility for long, mimicking regime-switching behaviour through a single-state mechanism.

Both the MS-GARCH and GARCH forecasts are smoothed using an exponentially weighted moving average with span 24 before comparison, to reduce short-term forecast noise and facilitate comparison of forecast dynamics.

**Table 3:** Volatility Forecast Quality: MS-GARCH vs. Causal GARCH(1,1)

Metric	GARCH(1,1)	MS-GARCH	Improvement
RMSE (smoothed)	0.037411	0.036711	−1.87%
Spearman IC (smoothed)	0.5264	0.5371	+1.07 pp
DM statistic		+4.7040	—
DM $p$ -value		$1.28 \times 10^{-6}$	—
Error mean	0.002324	0.001256	−46%
Error std	0.037339	0.036690	−1.74%

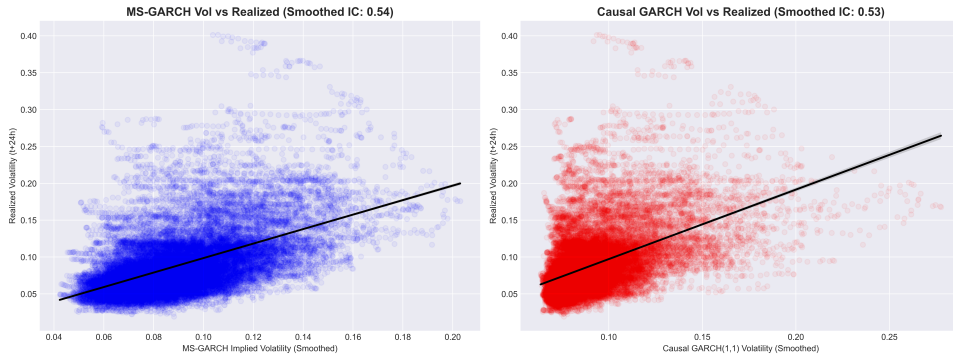


**Figure 1:** Realized vs. Implied Volatility Forecasts (Smoothed MS-GARCH vs. Causal GARCH)

The Diebold–Mariano test (Diebold and Mariano, 1995) formally confirms MS-GARCH superiority:  $DM = +4.7040$ ,  $p = 1.28 \times 10^{-6}$ , rejecting the null hypothesis of equal predictive accuracy at any conventional significance level. The higher smoothed IC of the MS-GARCH model reflects superior stability and regime-conditioned forecasting performance.

## 9. Empirical Results

### 9.1 Out-of-Sample Regime Allocations

The OOS regime allocations reflect the empirical distribution of EUR/USD microstructure states over the 2021–2025 period. At the 1D Macro scale, the model allocates 82.3% to Calm, 10.1% to Turbulent, and 7.7% to Crisis. At the 4H Meso scale, the allocation is 8.4% Calm, 71.6% Turbulent, and 20.0% Crisis. At the 1H Micro scale, the allocation is 65.6% Calm, 32.5% Turbulent, and 2.0% Crisis.

The striking divergence between timeframes is economically meaningful. The 1D model identifies the 2021–2025 period as predominantly calm at the macro level, consistent with the

daily timescale’s lower sensitivity to intraday noise. The 4H model identifies persistent turbulence (71.6%), reflecting the sustained institutional flow activity, elevated options market activity, and frequent ECB/Fed communication events that characterised this period. The 1H model’s 2.0% Crisis allocation reflects the rarity of genuine acute hourly stress episodes.

The Rolling Walk-Forward (WFA) quarterly analysis reveals substantial time-variation in regime allocations. In 2021-Q3 (July–September 2021), the 1D Macro model allocated 100% to Calm—a period of EUR/USD stability following the post-COVID recovery. In contrast, 2022-Q3 (July–September 2022) saw 77% Crisis allocation at the Macro level, corresponding to the peak of the Fed tightening cycle and EUR/USD falling below parity. This time-variation confirms that the model is capturing genuine regime dynamics rather than fitting a stationary mixture.

## 9.2 Conditional Return Profiles

**Table 4:** Conditional Return Profiles by Regime and Timescale (OOS: 2021–2025)

Timeframe	Regime	Ann. Vol	Fisher Kurtosis	OOS Alloc.
1D Macro	Calm	5.72%	1.0	82.3%
1D Macro	Turbulent	7.88%	4.4	10.1%
1D Macro	Crisis	13.45%	-0.7	7.7%
4H Meso	Calm	2.19%	0.2	8.4%
4H Meso	Turbulent	5.41%	3.0	71.6%
4H Meso	Crisis	13.22%	2.2	20.0%
1H Micro	Calm	3.70%	1.4	65.6%
1H Micro	Turbulent	10.92%	2.2	32.5%
1H Micro	Crisis	24.72%	3.2	2.0%

Some patterns emerge immediately from Table 4. First, the volatility ordering Calm < Turbulent < Crisis holds monotonically across all three timescales, confirming that no label switching has occurred. This is validated by Test 1 (OOS Volatility Stratification), which reports annualised volatilities of 3.70%, 10.92%, and 24.72% for the 1H Micro states.

## 9.3 OOS Regime Validation Diagnostics

**Table 5:** Out-of-Sample Regime Validation Results (Strategy-Independent, OOS 2021–2025)

Test	Result	Statistic
Test 1: Volatility Stratification	Calm < Turb < Crisis	Monotonic
Test 2: CVaR-99 Monotonicity	-32.3 < -49.9 < -55.9 bps	Monotonic
Test 3: OOS Churn Stability	4,365 flips / 24,955 hours	5.72h avg dwell
Test 4: KS Distributional Purity	Calm vs. Turb	$p = 1.35 \times 10^{-153}$
Test 4: KS Distributional Purity	Turb vs. Crisis	$p = 1.03 \times 10^{-38}$
Test 7: ACF Absorption	0.2579 → 0.1889	26.8% reduction
Test 8: Transition Stability	Empirical Calm persistence 0.876	—

The KS test results provide strong evidence that the three-state model has identified materially distinct market regimes, not arbitrary partitions of a homogeneous distribution.

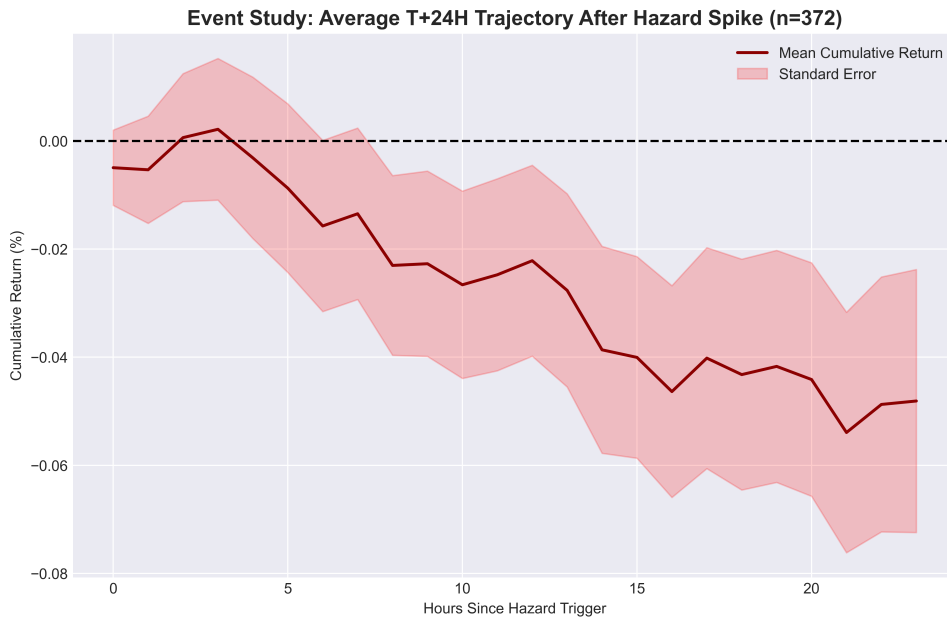


**Figure 2:** Average T+24H Trajectory After Hazard Spike

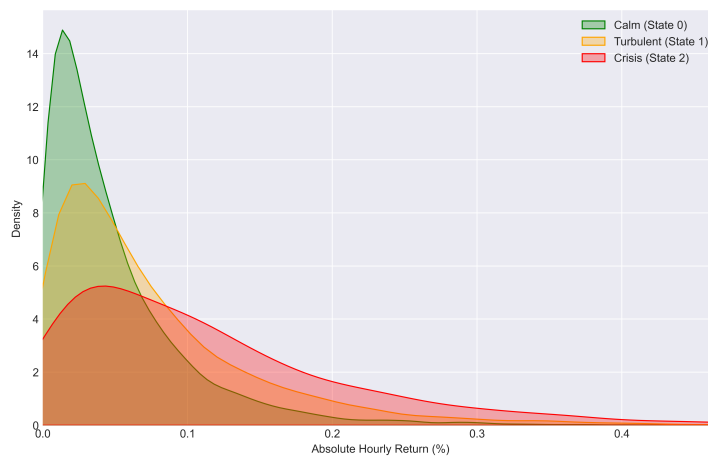


**Figure 3:** Out-of-Sample Return Distribution (1H) Separation Across Hidden States.

Kernel density estimates of absolute hourly returns for Calm, Turbulent, and Crisis regimes. The distributions progressively shift toward larger return magnitudes, supporting the volatility ordering observed across all temporal layers.

## 9.4 Three-Dimensional Volatility Tensor

To facilitate interpretation of the 27 joint state combinations, we group them into a small number of economically meaningful meta-regimes based on recurring cross-scale alignment patterns.

**Table 6:** Meta-Regime Attribution: WFA Rolling Results (2021–2025)

Meta-Regime Cluster	Dominant Tensor Configurations	Time Active	Mean IC
Synchronized Turbulence	1D:Turb · 4H:Turb · 1H:Turb	45.09%	+0.0312
Transitional Regime	Mixed Calm/Turb/Crisis states without full alignment	28.69%	+0.0330
Localized Micro Shock	1D:Calm · 4H:Calm · 1H:Crisis	13.55%	+0.0075
Macro Stress Divergence	1D:Crisis · 4H:Crisis · 1H:Calm	5.94%	+0.0544
Total Calm	1D:Calm · 4H:Calm · 1H:Calm	4.01%	-0.0226
Total Crisis	1D:Crisis · 4H:Crisis · 1H:Crisis	2.73%	-0.0436

The Macro Stress Divergence meta-regime (5.94% frequency) produces the highest IC (+0.0544), suggesting that cross-scale disagreement—macro and meso stress with micro calm—is associated with stronger predictive relationships. The Total Crisis meta-regime (2.73%) produces negative IC (-0.0436), suggesting that fully synchronised crisis conditions exhibit different predictive characteristics from cross-scale disagreement states.

## 9.5 Shannon Entropy Filter

The Shannon entropy measure provides a quantitative view of regime uncertainty. Lower entropy values correspond to more concentrated state probabilities and greater confidence in regime assignment, whereas higher entropy values indicate greater uncertainty and overlap between competing regime classifications. The quarterly entropy variation ranges from a minimum of 0.408 (2021-Q3, post-COVID calm with clear regime signals) to a maximum of 0.774 (2022-Q4, Fed pivot uncertainty creating ambiguous regime signals).

## 9.6 Formal Hypothesis Tests

**Table 7:** Formal Hypothesis Test Results

Hypothesis	Test	Statistic	$p$ -value
H1: MS-GARCH > GARCH	Diebold–Mariano	DM = +4.7040	$1.28 \times 10^{-6}$
H2: IC > 0.015, $p < 0.05$	IC significance test	IC = +0.0252	$6.75 \times 10^{-5}$

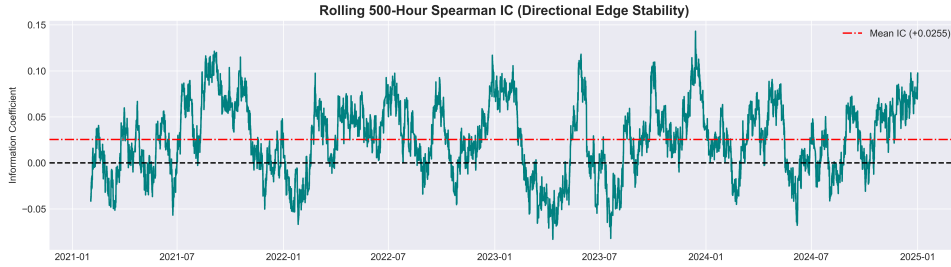


**Figure 4:** Rolling 500-Hour Spearman Information Coefficient (Directional Edge Stability)

## 10. Limitations and Future Research

### 10.1 Residual ARCH Effects

The ARCH-LM test (Engle, 1982) reveals statistically significant residual heteroskedasticity in all three timeframes (LM = 12.19,  $p = 0.032$  for 1D; LM = 16.75,  $p = 0.005$  for 4H; LM = 38.49,  $p = 0.000$  for 1H). The fundamental cause is the path-independence assumption of the Haas et al. (2004) specification: when the market transitions from Crisis back to Calm, the Calm GARCH variance immediately reverts to its unconditional level, ignoring the elevated volatility inherited from the Crisis state. This creates a discontinuity in the implied volatility path that manifests as residual ARCH in the standardised residuals.

The Gray (1996) path-dependent GARCH formulation addresses this by making the variance a function of the full history of filtered probabilities:  $\sigma_{t,k}^2 = \omega_k + \alpha_k \varepsilon_{t-1}^2 + \beta_k \mathbb{E}[\sigma_{t-1}^2 | r_{t-2}, \dots, r_1]$ , where  $\mathbb{E}[\sigma_{t-1}^2] = \sum_j \pi_{t-1}(j) \sigma_{t-1,j}^2$ . This “collapsing” approach ensures continuity across regime transitions but increases computational cost by a factor of 3–5.

### 10.2 RCM Value

RCM values of 27.6% (1D), 52.4% (4H), and 54.0% (1H). These indicate only moderate regime classification certainty. This reflects a fundamental challenge in FX regime modelling: the emission distributions of adjacent states overlap substantially. Unlike equity markets, where Calm and Crisis states have clearly separated return distributions driven by the leverage effect and volatility feedback, FX markets exhibit more continuous volatility dynamics. The Normal Inverse Gaussian distribution (Barndorff-Nielsen, 1997) and the Variance Gamma distribution (Madan et al., 1998) offer heavier tails and greater flexibility than the skew Student- $t$ , potentially improving regime separation by better fitting the extreme observations that define Crisis regimes.

### 10.3 Batch MLE: No Real-Time Adaptation

The current L-BFGS-B batch MLE approach re-estimates all parameters at each WFA quarter boundary, creating a computational bottleneck and preventing real-time parameter updating. Sequential Monte Carlo (particle filtering) methods would enable online parameter estimation, allowing the model to adapt continuously to changing market conditions. The particle filter maintains a particle approximation to the joint posterior  $P(\theta, S_t | r_1, \dots, r_t)$  and can detect

structural breaks in real time through the effective sample size (ESS) criterion.

#### 10.4 Univariate Framework

The current framework models EUR/USD in isolation. FX correlations spike during crisis regimes—a feature that the univariate MS-GARCH model cannot capture. A multivariate extension using regime-switching copulas would capture cross-asset contagion dynamics, providing richer signals for the TVTP drivers and more robust crisis detection. The joint emission density under a regime-switching copula is  $f(r_t | S_t = k) = c_k(F_{1,k}(r_{1,t}), \dots, F_{n,k}(r_{n,t})) \cdot \prod_i f_{i,k}(r_{i,t})$ , where  $c_k$  is the state-conditional copula.

#### 10.5 Markov Assumption and Duration Dependence

The first-order Markov assumption implies that regime transitions depend only on the current state, not on how long the system has been in that state. Durland and McCurdy (1994) documented empirical evidence of duration dependence in US GNP growth regimes, motivating semi-Markov models in which transition probabilities depend on regime age. For EUR/USD, there is economic reason to expect duration dependence: a Calm regime that has persisted for 60 days may be more likely to transition than one that has persisted for only 5 days, as the longer-duration calm may reflect a structural equilibrium that is more resistant to perturbation.

#### 10.6 Single Currency Pair

The framework is validated exclusively on EUR/USD. Generalisation to other major pairs (GBP/USD, USD/JPY, USD/CHF) and emerging market currencies would test the robustness of the triple-timeframe architecture and the universality of the identified regime structure. Different currency pairs may require different stickiness priors, TVTP driver compositions, and parameter bounds.

### 11. Conclusion

This paper has introduced a triple-timeframe Markov-Switching GARCH framework with time-varying transition probabilities for volatility regime detection in EUR/USD. The framework makes three core contributions: a multi-scale architecture that resolves the fundamental scale mismatch problem of single-timeframe HMMs; TVTP driven by composite microstructure stress indices with decisive AIC improvements of +690.7 (4H) and +499.9 (1H) (Akaike, 1974); and a 27-dimensional joint probability tensor enabling cross-scale interaction analysis through a Mixture-of-Experts routing architecture.

The empirical results provide evidence that the proposed framework improves volatility forecasting accuracy and produces economically interpretable regime structures. The Diebold–Mariano test (Diebold and Mariano, 1995) confirms statistically superior volatility forecasting:  $DM = +4.7040$  ( $p = 1.28 \times 10^{-6}$ ). The KS distributional purity test confirms that the three

regimes represent genuinely distinct data-generating processes:  $p = 1.35 \times 10^{-153}$  for Calm vs. Turbulent. The master directional IC of  $+0.0252$  ( $p = 6.75 \times 10^{-5}$ ) confirms statistically significant directional predictability.

The empirical results support the central thesis that volatility dynamics in EUR/USD are inherently multi-scale and regime-dependent. The proposed framework produces statistically distinct volatility states, improving volatility forecasting accuracy relative to a single-regime GARCH benchmark, and captures meaningful interactions across temporal layers through the joint probability tensor. These findings suggest that modelling volatility as a hierarchy of interacting regimes provides a richer representation of market dynamics than conventional single-timescale approaches.

The path forward is clear. NIG or VG emissions (Barndorff-Nielsen, 1997; Madan et al., 1998) would improve regime separation by better fitting the extreme observations that define Crisis regimes. Particle filtering would enable online parameter estimation and real-time structural break detection. Regime-switching copulas would extend the framework to multivariate settings, capturing cross-asset contagion dynamics. Semi-Markov models (Durland and McCurdy, 1994) would address the duration dependence limitation of the first-order Markov assumption. Each of these extensions addresses a specific, quantified limitation of the current framework, providing a clear research agenda for future work.

## References

- Barndorff-Nielsen, O. E. (1997). Normal inverse Gaussian distributions and stochastic volatility modelling. *Scandinavian Journal of Statistics*, 24(1), 1-13.
- Bollerslev, T. (1986). Generalized autoregressive conditional heteroskedasticity. *Journal of Econometrics*, 31(3), 307-327.
- Brier, G. W. (1950). Verification of forecasts expressed in terms of probability. *Monthly Weather Review*, 78(1), 1-3.
- Diebold, F. X., & Mariano, R. S. (1995). Comparing predictive accuracy. *Journal of Business & Economic Statistics*, 13(3), 253-263.
- Durland, J. M., & McCurdy, T. H. (1994). Duration-dependent transitions in a Markov model of US GNP growth. *Journal of Business & Economic Statistics*, 12(3), 279-288.
- Engle, R. F. (1982). Autoregressive conditional heteroscedasticity with estimates of the variance of United Kingdom inflation. *Econometrica*, 50(4), 987-1007.
- Filardo, A. J. (1994). Business-cycle phases and their transitional dynamics. *Journal of Business & Economic Statistics*, 12(3), 299-308.
- Gray, S. F. (1996). Modeling the conditional distribution of interest rates as a regime-switching process. *Journal of Financial Economics*, 42(1), 27-62.

- Haas, M., Mittnik, S., & Paoletta, M. S. (2004). A new approach to Markov-switching GARCH models. *Journal of Financial Econometrics*, 2(4), 493-530.
- Hamilton, J. D. (1989). A new approach to the economic analysis of nonstationary time series and the business cycle. *Econometrica*, 57(2), 357-384.
- Madan, D. B., Carr, P. P., & Chang, E. C. (1998). The variance gamma process and option pricing. *European Finance Review*, 2(1), 79-105.
- Akaike, H. (1974). A new look at the statistical model identification. *IEEE Transactions on Automatic Control*, 19(6), 716-723.
- Shannon, C. E. (1948). A mathematical theory of communication. *Bell System Technical Journal*, 27(3), 379-423.
- Kolmogorov, A. (1933). Sulla determinazione empirica di una legge di distribuzione. *Giornale dell'Istituto Italiano degli Attuari*, 4, 83-91.

## A. Key Model Parameters and Diagnostic Statistics

**Table 8:** Summary of Key Model Parameters and Diagnostic Statistics (OOS: 2021–2025)

Diagnostic / Statistic	1D Macro	4H Meso	1H Micro
AIC	+2170.24	−6880.72	−80160.25
TVTP Justified?	No (static)	Yes ( $\Delta\text{AIC} = +690.7$ )	Yes ( $\Delta\text{AIC} = +499.9$ )
Calm Dwell Time	45.1 days	10.8 days	10.7 hours
Turbulent Dwell Time	13.9 days	1.9 days	5.1 hours
Crisis Dwell Time	7.6 days	0.6 days	3.9 hours
Brier Skill Score	+0.2132	+0.0874	+0.1185
RCM Clarity	27.6%	52.4%	54.0%
ARCH-LM $p$ -value	0.0323	0.0050	0.0000
Calm→Calm Persistence	0.9778	0.9846	0.9062
Crisis→Crisis Persistence	0.8685	0.7282	0.7440
OOS Calm Allocation	82.3%	8.4%	65.6%
OOS Turbulent Allocation	10.1%	71.6%	32.5%
OOS Crisis Allocation	7.7%	20.0%	2.0%

## B. Formal Hypothesis Test Results

**Table 9:** Formal Hypothesis Test Results (Phase 8)

Hypothesis	Test	Statistic	$p$ -value
H1: MS-GARCH > GARCH	Diebold–Mariano	DM = +4.7040	$1.28 \times 10^{-6}$
H2: IC > 0.015, $p < 0.05$	IC significance test	IC = +0.0252	$6.75 \times 10^{-5}$

### C. WFA Quarterly Scorecard

**Table 10:** Selected WFA Quarterly Results (2021-Q1 through 2024-Q4)

Quarter	IC	Macro Alloc. (Calm/Turb./Crisis)	Micro RCM	Avg Entropy	Avg Confidence
2021-Q1	-0.0052	4%/39%/57%	47%	0.593	0.743
2021-Q2	+0.0105	29%/71%/0%	53%	0.530	0.775
2021-Q3	+0.0699	100%/0%/0%	66%	0.408	0.841
2021-Q4	+0.0126	19%/80%/1%	61%	0.449	0.818
2022-Q1	+0.0183	38%/0%/62%	46%	0.588	0.728
2022-Q2	+0.0531	23%/1%/76%	37%	0.687	0.684
2022-Q3	+0.0284	6%/16%/77%	38%	0.696	0.699
2022-Q4	+0.0351	24%/61%/15%	29%	0.774	0.637
2023-Q1	-0.0027	38%/60%/3%	41%	0.639	0.706
2023-Q2	+0.0141	88%/12%/0%	47%	0.605	0.745
2023-Q3	+0.0167	15%/71%/14%	48%	0.576	0.750
2023-Q4	+0.0328	26%/0%/74%	46%	0.613	0.737
2024-Q1	+0.0219	56%/39%/5%	50%	0.564	0.766
2024-Q2	+0.0209	81%/15%/4%	58%	0.477	0.803
2024-Q3	+0.0107	86%/0%/14%	54%	0.517	0.782
2024-Q4	+0.0663	13%/27%/61%	45%	0.618	0.730
Mean	<b>+0.0252</b>	—	—	—	—